Journal of Materials Chemistry A

Accepted Manuscript

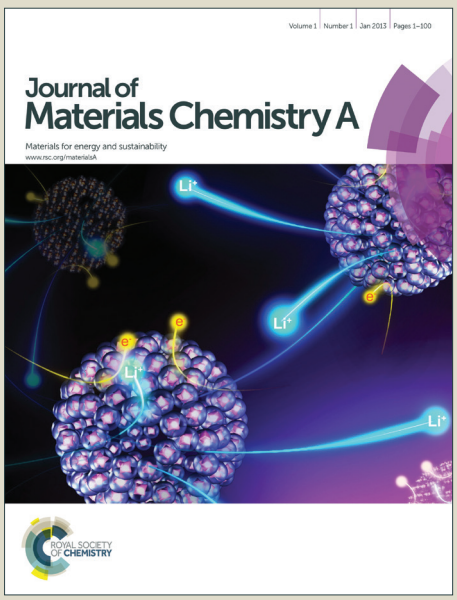

ROYAL SOCIETY OF CHEMISTRY

www.rsc.org/materialsA

Journal Name

COMMUNICATION

Highly efficient planar perovskite solar cells with a TiO_2/ZnO electron transport bilayer

Received 00th January 20xx,
Accepted 00th January 20xx

DOI: 10.1039/x0xx00000x

www.rsc.org/

Xin Xu[a], Huiyin Zhang[a], Jiangjian Shi[a], Juan Dong[a], Yanhong Luo[a], Dongmei Li[a] and Qingbo Meng[a,†]

A TiO_2/ZnO electron transport bilayer, which combines the advantages in high electron extraction and low interfacial recombination together, has been designed for the planar perovskite solar cell. With this bilayer, the front surface recombination in the cell is significantly suppressed, and a high efficiency exceeding 17% has been achieved. These results suggest a promising and simple approach to further design the photovoltaic devices from the aspect of charge transport and recombination.

Perovskite organic lead halide compounds have attracted more and more attention as light absorber for the thin-film solar cell, due to their high light absorption, long carrier diffusion length and low-cost fabrication technologies[1-7]. Numerous of works has been reported to improve the device performance in a short period of time[8-13], and the highest power conversion efficiency (PCE) of 20.1% was certified. For perovskite solar cells, different device structures including mesoscopic[11], planar[12], inverted[14] and single-heterojunction[15, 16] have demonstrated to be promising for high efficiency. No matter what kind of device structures, high-quality perovskite absorber and excellent interface properties are always crucial to the cell performance, typically to efficient charge carrier generation, collection and suppressing the recombination in perovskite solar cells[17-20]. As for planar structure devices, the electron transport layer (ETL) plays a dramatic role in charge separation and transport, eliminating the electrical shunts between the transparent electrode/perovskite and transparent electrode/hole transport material (HTM) interfaces[21-23]. Therefore, a dense, pin-hole free and well electrically conductive electron transport layer is highly demanded for well performed planar perovskite solar cells.

ZnO, with many merits such as good transparency in the visible spectrum, high electron mobility and various nanostructures[24-26], is supposed to be an ideal choice as ETL for this cell. Some methods have been developed to prepare compact ZnO layers, such as deposition from nanoparticle suspension[27], atomic layer deposition (ALD)[28] and magnetron sputtering (MS) methods[29], yielding a relative high performance. However, these processes are relatively complicated, such as well dispersive nanoparticles are needed or expensive cost in ALD or MS equipment are required, which may be disadvantageous to widespread application. In fact, spin coating of ZnO precursor sol-gel solution is a simple, low-cost and fast way to approach ETL[30]. However, this sol-gel ZnO layer is still suffering from some inadequacies, for example, thermal treatment will introduce cracks[30]. These cracks may lead to the direct contact of perovskite absorber and electrode, reducing the blocking effect of ETL. Moreover, serious charge recombination and energy level offset usually occur in the ZnO/perovskite interface, limiting the further improvement in the cell performance[31-33]. On the other way, TiO_2, as widely used ETL in planar perovskite solar cells, suggested to exhibit good blocking effect for high-efficiency devices[23]. However, electron collection and transport may be less effective in TiO_2, leading to great hysteresis which is mentioned in other researches[34, 35]. Thus, new investigations on a better performed electron transport layer from this facile fabrication method are still needed to enhance the power-conversion of planar perovskite solar cells.

In this work, we developed a TiO_2/ZnO bilayer by sol-gel method as the electron transport layer for the planar perovskite solar cell. This kind of bilayer can produce a more compact interfacial layer, which will avoid the direct contact between SnO_2: F (FTO) electrode and perovskite absorber. The X-ray photoelectron spectra results reveals that the energy level structure of FTO/TiO_2/ZnO/perovskite absorber helps to transport the photo-induced carriers, avoiding charge accumulation to reduce recombination. Current-voltage, transient photovoltage and impedance spectra results demonstrate that the charge recombination in the cell is significantly suppressed. Finally, the cell efficiency is promoted from 13.2% to 17.2%, indicating a solid improvement in cell performance with this interfacial bilayer.

[a] *Key Laboratory for Renewable Energy (CAS), Beijing Key Laboratory for New Energy Materials and Devices, Beijing National Laboratory for Condense Matter Physics, Institute of Physics, Chinese Academy of Sciences, Beijing 100190, China.*
† Corresponding author: 86-10-8264 9242. Email address: qbmeng@iphy.ac.cn.
Electronic Supplementary Information (ESI) available: DOI: 10.1039/x0xx00000x

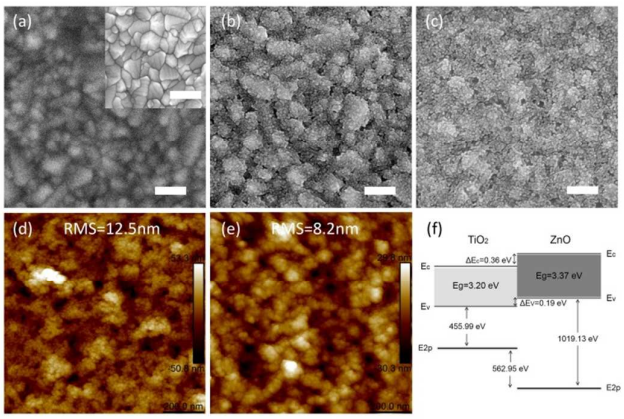

Fig.1 (a) Top-view SEM images of the compact layers composing of TiO_2 (inset is the bare FTO substrate), (b) ZnO and (c) TiO_2/ZnO bilayer on the FTO substrates.. Scale bar: 200nm. AFM height images of ZnO film (d) and TiO_2/ZnO film (e) (1μm×1μm) and (f) the energy diagram of TiO_2/ZnO bilayer.

Results and discussions

The morphology of the ETLs composing of TiO_2 or ZnO single layer and TiO_2/ZnO bilayer, respectively, is shown in Figure 1. As seen in Figure 1(a), the morphology of FTO polycrystalline can still be distinguished after being covered with a thin TiO_2 layer, which implies that the TiO_2 layer is thin enough. However, this TiO_2 layer shows an amorphous-like morphology and poor conductivity, in agreement with the previous work[23]. On the contrary, the ZnO layer on the FTO substrate deposited by sol-gel method with hydrolysis of the precursor solution shows a clearer feature of aggregated nanoparticles and a better conductivity, as in Figure 1(b). On the other hand, these nanoparticles are supposed to give a high interface area between ZnO and perovskite absorber for charge extraction, and the high conductivity is beneficial for electron transport[36]. However, some large pin holes can be clearly seen between the aggregations, which will lead to the direct contact between perovskite absorber and the FTO electrode, causing serious recombination. To TiO_2/ZnO compact bilayer, no FTO substrate is directly observed, and meanwhile less pin holes on the surface is found, as shown in Figure 1(c). The XRD pattern of different ETL is give in Figure S1, *Supplementary Information*. Obviously, this compact ZnO layer with a thin TiO_2 layer underneath is expected to avoid the direct contact between the perovskite absorber and the FTO electrode. In addition, the surface of the TiO_2/ZnO compact bilayer is smooth with reduced pin-holes in some scale. This was confirmed by the AFM measurement results that the TiO_2/ZnO bilayer films exhibited smaller surface roughness (RMS=8.2nm, Figure 1(e)) than the ZnO films (RMS=12.5nm, Figure 1(d)).

Moreover, XPS measurement results reveal that the valence band maximum and conduction band minimum of ZnO are a little higher than those of TiO_2 (ΔE_V=0.19eV), thus suggesting that the TiO_2/ZnO bilayer has a type-II energy band structure, which is in agreement with Figure 1(f)[37-39]. More details could be seen in the Supplementary Materials (Figure S2). This energy band structure could help electron transportation at TiO_2/ZnO interface, and suppress charge accumulation in the ZnO layer and the recombination at ZnO/perovskite absorber interface[40]. The combined TiO_2-ZnO system was also reported in Dye-sensitized solar cells (DSSCs) previously. A. Agrios et al used ZnO/TiO_2 nanocomposite films to increase surface area and improve electron transport for high efficiency DSSCs[41]. In the meantime, this composite may suffer from an energy barrier when the TiO_2 is on the top of the ZnO, which may limit the electron transfer. On the contrary, when the TiO_2 is under the ZnO layer, the generated electrons can be easily injected due to the band alignment, which also agrees with other researches[42, 43].

With this ETL, the planar perovskite solar cells with a structure as shown in Figure 2(a) are fabricated. The TiO_2/ZnO electron transport bilayer is covered on the FTO substrate. A uniform and dense perovskite absorber with a thickness of about 300 nm is deposited on the ETL, and is smoothly covered with a 300 nm-thick spiro-OMeTAD as the hole transport layer (HTL). Then the Au back electrode with a thickness of about 80 nm is finally evaporated contacting with the HTL, benefiting for interfacial charge transport. The perovskite layer was made by a fast crystallization-deposition method which was firstly reported by Xiao *et al.*[44] A very smooth surface and high quality crystals are obtained for the perovskite layer prepared by this method (Figure 2c). Free charge carriers generated in the perovskite absorber layer under illumination can be extracted by the electron selective contact and hole-transporting material, based on the energy levers of each device components (Figure 2b).

Since the thickness of ETL can play an important role in planar perovskite solar cells, we fabricated devices with different thickness ZnO, TiO_2/ZnO ETL to find the final optimized component. For the devices only using ZnO as ETL, It can be seen that (Table S1, *Supplementary Information*) when the ZnO is 20nm, the devices exhibit bad performances with low open-circuit voltages and fill factors. The power-conversion efficiency began to increase with ETL thickness increasing. But when an 80nm-thick ETL is used, the efficiency became to decrease again due to the reduced fill factors. After optimization, we found the 50nm-thick ZnO layer ETL device performed the best. It also can be concluded that merely increasing ETL thickness cannot further improve the performance of planar perovskite solar cells. Therefore, more efficient modification should be developed. When a thin layer of TiO_2 is added under the ZnO, the performance of devices is dramatically improved. Different thickness was also optimized (Table S2, *Supplementary Information*) and the best performance can be achieved with TiO_2/ZnO around 10nm/50nm. We will start the following discussion based on the optimal results.

Figure 2(d) presents the current-voltage (*I-V*) results of the cells with different ETLs. We can see that, the TiO_2/ZnO device exhibits well *I-V* performances, with short-circuit current density (J_{SC}) of 20.12 mA cm^{-2}, open-circuit voltage (V_{OC}) of 1084.7 mV, fill factor (FF) of 0.753 and power-conversion efficiency (PCE) of 16.44%. The bare ZnO ETL device shows a

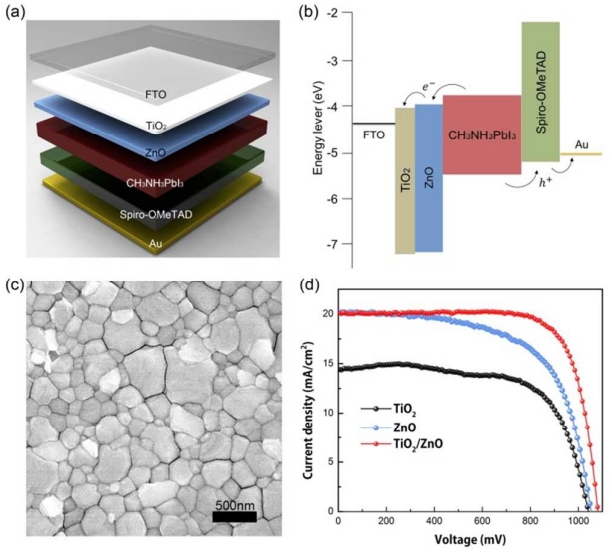

Fig.2 Schematic diagrams of the (a) device structure, (b) energy levels, and (c) perovskite surface morphology SEM image, and (d) current-voltage curves of the planar perovskite solar cell.

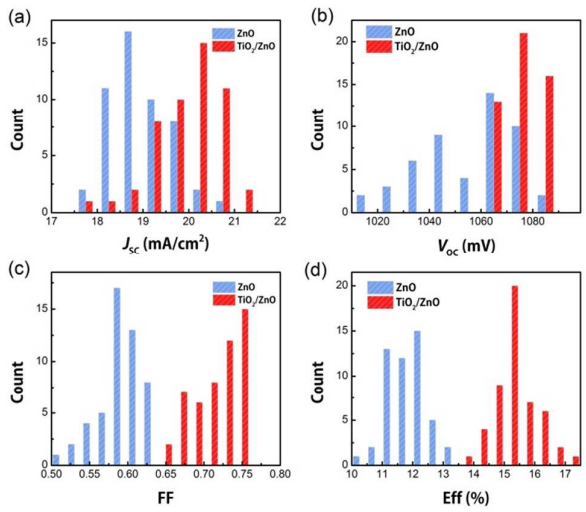

Fig.3 Histograms of performance with (a) J_{SC}, (b) V_{OC}, (c) fill factor and (d) PCE for the cells with ZnO single layer and TiO_2/ZnO bilayer as the compact layers, respectively. Fifty cells for each condition are involved in this statistics.

relatively less performances, mainly due to the reduced V_{OC} and fill factor. The significant differences in film morphology as discussed in Figure 1 can be one of the origins. In addition, the *I-V* curve of the TiO_2/ZnO bilayer based cell can be well described with a single diode model, agreeing with the semiconductor theory[45]. On the contrary, a serious charge recombination is estimated from the *I-V* curve of the ZnO based cell. This *I-V* curve cannot be described by a single diode model, but can be well fitted with a parallel-connected double diode model (Figure S3)[45]. This result indicates that part of the $CH_3NH_3PbI_3$ absorber may contact directly with the FTO electrode, forming a shunt diode of serious recombination. Thus, it can be concluded that the shunt recombination at FTO/$CH_3NH_3PbI_3$ absorber interface has been significantly suppressed with the additional TiO_2 layer as expected. Moreover, we presented the device only with spin coating TiO_2 ETL for comparison. A low short-circuit current density (J_{SC}) of 14.5 mA cm^{-2} is achieved probably due to the poor charge extraction at TiO_2/perovskite absorber interface. A strange bending between 0 and 600 mV exists in the *I-V* curve with serious hysteresis (forward PCE of 2.1% and backward of 10.2%, Figure S4, *Supplementary Information*), implying charge accumulation at interfaces and slow charge extraction. Some researches[34] suggested that compact TiO_2 used in planar perovskite solar cells can exhibit great hysteresis and the electron collection on the TiO_2/perovskite interface may be less efficient. These results indicate that electron extraction at the ZnO/$CH_3NH_3PbI_3$ interface is more effective than that at the TiO_2/$CH_3NH_3PbI_3$ interface. Furthermore, the comparison of performance between the cells with ZnO and TiO_2/ZnO compact layers is statistically analyzed with the histograms, as shown in Figure 3. It is unambiguous that the cell performance can be significantly enhanced with the design of the compact bilayer.

With this design and optimizations on cell fabrication, high efficiencies for the planar perovskite solar cell with ZnO/$CH_3NH_3PbI_3$ acting as the electron extraction interface are obtained. The *I-V* results of the best performed cell are shown in Figure 4(a). A PCE of 16.1% with J_{SC} of 20.8 mA cm^{-2}, V_{OC} of 1084 mV and FF of 0.714 (forward: 15.0%, backward: 17.2%) is achieved according to the average *I-V* curve. The external quantum efficiency (EQE) of this cell is also shown in Figure 4(b), integration of which yielding a J_{SC} of 20.05 mA cm^{-2}, agreeing well with the *I-V* result. Further perspective of *I-V* curves of TiO_2/ZnO ETL perovskite solar cells under different scan rate is given in Figure S5. The stabilities of devices based on TiO_2, ZnO and TiO_2/ZnO are also compared in Figure S6. All the devices presented continuous decline of PCEs. This might due to the instability of spiro-OMeTAD as hole transport material. After two weeks, the TiO_2/ZnO devices still exhibit better performance than the ZnO or TiO_2 ones. However, compared to TiO_2 ETL devices, the ZnO based solar cells

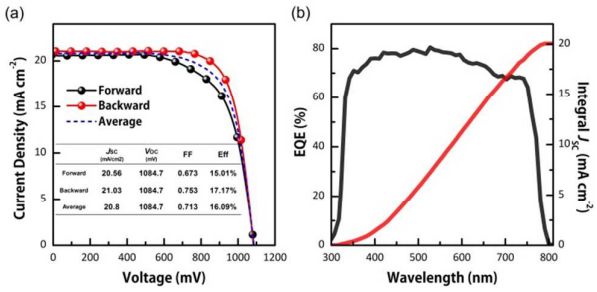

Fig.4 (a) Current-voltage (forward scan: from short circuit to forward bias. backward scan: from forward bias to short circuit. Scan rate: 100mV/s, delay time 100ms, and (b) external quantum efficiency (EQE) results of the best performed cell.

presented the less stability probably caused by chemical reaction on the ZnO interface[46]. Therefore, it still need more research to help to give better understanding and to enhance the stability of ZnO ETL perovskite solar cells.

To further clarify the origins of this enhancement with the TiO_2/ZnO bilayer compared to the ZnO single compact layer, the dark *I-V* curves are analyzed to investigate the charge recombination properties in the cells. As the dark *I-V* curves shown in Figure 5(a), both of the devices keep nearly zero before 500mV. However, the ZnO ETL devices exhibit a rapid drop after 600mV, whereas the devices with TiO_2 interlayer begin to fall off at around 900mV. Further calculations[15] imply that the equivalent saturated current density of the ZnO single layer based cell (6.8×10^{-7} mA cm^{-2}) is hundred times larger than that of the TiO_2/ZnO bilayer based cell (7.6×10^{-9} mA cm^{-2}). The improved dark current and reduced revise saturated current density of TiO_2/ZnO bilayer devices indicate that the TiO_2/ZnO bilayer has a better blocking effect result in reduced recombination process, which is effective to improve fill factor and V_{OC}, and better performances of planar perovskite solar cells.

Transient photovoltage spectroscopy (TPV) methods[47] are proposed to study the transport and recombination process of charge carriers in the devices. The TPV results shown in Figure 5(b) indicate that the charge recombination velocity of the TiO_2/ZnO based cell is much slower than that of the ZnO based cell. It also can be seen that the charge transport velocity of the cell is somewhat slowed due to the additional TiO_2 layer, as shown with the transient photocurrent result in the inset of Figure 5(b).

The differences in the charge recombination of these cells are further confirmed by the impedance spectra[48, 49] results. In the Nqyuist plots of both the ZnO and the TiO_2/ZnO based cells, semicircles can be observed in the intermediate frequency region, as inset of Figure 5(c) shows, which are related to the charge transfer at FTO/compact/perovskite/HTL interface. The charge transfer resistance (R_{CT}) of the cell can be derived with fitting the Nyquist plots with a resistance-constant phase element model (*R-CPE*). As can be seen in Figure 5(c), the R_{CT} of the TiO_2/ZnO based cell is obviously larger than that of the ZnO based cell, agreeing well with other results discussed above. Therefore, it is concluded that the charge recombination in the planar perovskite solar cell has been significantly suppressed with the design of TiO_2/ZnO electron transport bilayer.

For a better understanding into the origins discussed above, the schematic diagrams of charge transport and recombination in the cell are depicted in Figure 6. As large pin holes exist in the ZnO compact layer, the perovskite absorber can infiltrate into these holes and contact directly with the FTO electrode, as shown in Figure 6(a). In this Schottky contact, the free electron is easy to re-inject into the valence band of the perovskite absorber due to a low interfacial energy barrier, causing serious front surface recombination. Moreover, carrier depletion can exist in the ZnO layer due to the mismatch in the work functions between FTO and ZnO[13], which will affect the smooth electron transport in the ZnO layer, causing charge accumulation and recombination at ZnO/perovskite absorber interface. On the other hand, when the thin TiO_2 layer is introduced, the direct contact between FTO and perovskite absorber can be effectively eliminated. Moreover, the band offset at the TiO_2/ZnO interface can further help electron injection and transfer in the ETLs, and lower the recombination at the ZnO/perovskite interface as well. Thus, the overall charge recombination in the cell is suppressed, and the cell performance is significantly enhanced.

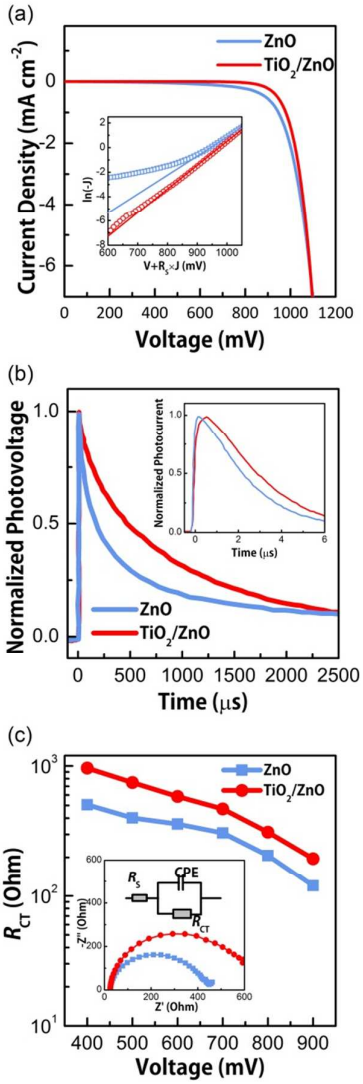

Fig.5 (a) Dark current (inset: fitting with diode model), (b) transient photovoltage (inset: transient photocurrent) and (c) charge transfer resistance (inset: Nyquist plots of the cells at 600 mV under 0.2 sun) results of the cells with ZnO single layer and TiO_2/ZnO bilayer as the compact layers, respectively.

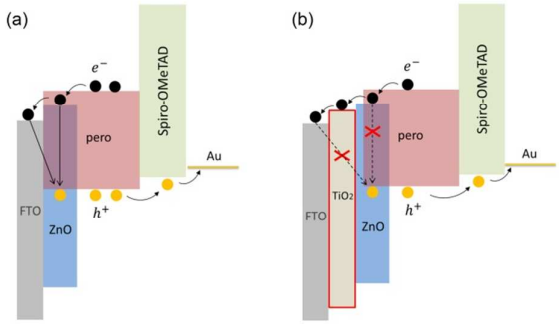

Fig.6 Schematic diagrams of band alignment and charge recombination in the cells with (a) ZnO single layer and (b) TiO_2/ZnO bilayer as the compact layers, respectively.

Experiment details

Materials

PbI_2 was purchased from Aldrich-Sigma (99.8%), N, N-dimethylformamide (DMF) and chlorobenzene from Alfar Aesar. Isopropanol was purchased from J&K Chemicals. Zinc acetate dihydrate (AR, 99.0%), hydroiodic acid (AR, 45 wt% in water) and methylamine (AR, 27% in methanol) from Sinopharm Chemical Reagent Co. Ltd. CH_3NH_3I was synthesized according to the literature[9]. Spiro-OMeTAD was from Luminescence Technology Corp., Taiwan. All the chemicals were directly used without further purification.

Device fabrication

Laser-patterned FTO glass (Pilkington, thickness of 2.2 mm and sheet resistance of 15 Ω/sq) was sequentially cleaned with mild detergent, distilled water and ethanol in an ultrasonic bath. After dried with air stream, they were treated by ultraviolet ozone (UVO) for 15 minutes to remove organic materials. For the ZnO ETL, a 50 nm-thick ZnO layer was spin coated onto the FTO substrate with $Zn(Ac)_2$ solution in methanol (0.25M, 3000 rpm, 20s), and followed by thermal treatment at 350 °C for 30 minutes. For the TiO_2/ZnO ETL, a TiO_2 thin layer (10 nm) was firstly spin coated (4000rpm) onto the FTO substrate with titanium (IV) isopropoxide solution in ethanol (0.14M) as the precursor and with 500°C thermal treatment for 30min before depositing the ZnO layer.The $CH_3NH_3PbI_3$ layer was deposited by a fast deposition-crystallization procedure according to the literature[44]. 30 µl perovskite precursor solution (equimolar PbI_2 and CH_3NH_3I dissolved in DMF, 45wt%) was first dropped onto the prepared ETL film. After the substrate spun at 5000 rpm for six seconds, anhydrous chlorobenzene (100ul) was poured on the center of the substrate to induce quickly crystallization of the perovskite. The obtained films were dried on a hot plate at 90 °C for 10 minutes. After that, a 300 nm-thickness hole transport layer composing of spiro-OMeTAD in chlorobenzene was spin coated (2000rpm) on the perovskite films. The preparation of perovskite films and HTLs were carried out in a N_2-filled glove box. Finally, an 80 nm-thick gold back electrode was deposited onto the above prepared films by thermally evaporation (Kurt J. Lesker).

Characterization

Film thickness of the films was measured by a surface profiler (KLA-Tencor). The morphologies of the films were obtained with scanning electron microscopy (SEM, Hitachi S4800) at 10kV acceleration voltage. Atomic force microscope (AFM) height images were obtained with Bruker Multmode 8 AFM using ScanAsyst mode. X-ray photoelectron spectroscopy (XPS) was performed on the Thermo Scientific ESCALab 250Xi using 200 W monochromated Al Kα radiation. The 500 µm X-ray spot was used for XPS analysis. The base pressure in the analysis chamber was about 3×10^{-10} mbar. Typically the hydrocarbon C1s line at 284.8 eV from adventitious carbon is used for energy referencing. For the current-voltage (*I-V*) measurements, the cells were illuminated under AM 1.5 simulated sunlight (100 mW/cm^2) from Oriel Solar Simulator 91192. *I-V* curves were recorded by a digital source meter (Keithley model 2602). The solar cells were masked with a black aperture to define the active area of 0.1 cm^2. The *I-V* scan rate was 100mV/s with a delay time of 100ms at each point. External quantum efficiency (EQE) of the cells was measured with a lab-made IPCE setup. Transient photovoltage/current were obtained recorded by a sub-nanosecond resolved digital oscilloscope (Tektronix DPO 7104) with input impedances of 1 MΩ and 50Ω, respectively, after the cell was excited by a pulsed double frequency Nd:YAG laser (Brio, 20 Hz, 4 ns) at 532 nm with an ultralow light intensity. Impedance spectra measurements were performed with an IM6ex electrochemical workstation (Zahner) under 0.2 sun illumination at positive bias voltages ranging from 0.4 to 0.9 V in the range of 1 M~0.5 Hz with a perturbation amplitude of 10 mV.

Conclusions

A TiO_2/ZnO electron transport bilayer, which combines the advantages of high electron extraction and low interfacial recombination together, has been applied for the planar perovskite solar cell. This bilayer together with the perovskite absorber forms a type-II energy band structure, benefiting for electron transport and avoiding charge accumulation. Moreover, this kind of ETL can effectively eliminate the direct contact between FTO electrode and the perovskite absorber. Due to these advantages, the front surface recombination in the cell is significantly suppressed, and a high efficiency exceeding 17% has been achieved. This modified structure of electron transport layer is proved to be an effect approach to further improve the performance of perovskite solar cells.

Acknowledgement

The authors would like to acknowledge the financial support from the MOST (973 projects, No. 2012CB932903 and 2012CB932904), NSFC (Nos. 51402348, 11474333, 91433205,

51421002, 91233202and 21173260) and the Knowledge Innovation Program of the Chinese Academy of Sciences. The author would also thank Dr. Xiang Hao from Institute of Chemistry, Chinese Academy of Sciences for the help in the GIXRD measurement.

References

1. S. D. Stranks, G. E. Eperon, G. Grancini, C. Menelaou, M. J. P. Alcocer, T. Leijtens, L. M. Herz, A. Petrozza and H. J. Snaith, *Science*, 2013, **342**, 341-344.
2. G. Xing, N. Mathews, S. Sun, S. S. Lim, Y. M. Lam, M. Grätzel, S. Mhaisalkar and T. C. Sum, *Science*, 2013, **342**, 344-347.
3. T. Baikie, Y. Fang, J. M. Kadro, M. Schreyer, F. Wei, S. G. Mhaisalkar, M. Graetzel and T. J. White, *J. Mater. Chem. A*, 2013, **1**, 5628-5641.
4. P. Gao, M. Gratzel and M. K. Nazeeruddin, *Energy Environ. Sci.*, 2014, **7**, 2448-2463.
5. H.-S. Kim, S. H. Im and N.-G. Park, *J. Phys. Chem. C*, 2014, **118**, 5615-5625.
6. H. J. Snaith, *J. Phys. Chem. Lett.*, 2013, **4**, 3623-3630.
7. M. A. Green, A. Ho-Baillie and H. J. Snaith, *Nat. Photonics*, 2014, **8**, 506-514.
8. A. Kojima, K. Teshima, Y. Shirai and T. Miyasaka, *J. Am. Chem. Soc.*, 2009, **131**, 6050-6051.
9. J. Burschka, N. Pellet, S.-J. Moon, R. Humphry-Baker, P. Gao, M. K. Nazeeruddin and M. Gratzel, *Nature*, 2013, **499**, 316-319.
10. N. J. Jeon, J. H. Noh, Y. C. Kim, W. S. Yang, S. Ryu and S. I. Seok, *Nat. Mater.*, 2014, **13**, 897-903.
11. H.-S. Kim, C.-R. Lee, J.-H. Im, K.-B. Lee, T. Moehl, A. Marchioro, S.-J. Moon, R. Humphry-Baker, J.-H. Yum, J. E. Moser, M. Grätzel and N.-G. Park, *Sci Rep*, 2012, **2**, 591.
12. M. Liu, M. B. Johnston and H. J. Snaith, *Nature*, 2013, **501**, 395-398.
13. H. Zhou, Q. Chen, G. Li, S. Luo, T.-b. Song, H.-S. Duan, Z. Hong, J. You, Y. Liu and Y. Yang, *Science*, 2014, **345**, 542-546.
14. Z. Xiao, Q. Dong, C. Bi, Y. Shao, Y. Yuan and J. Huang, *Adv. Mater.*, 2014, **26**, 6503-6509.
15. J. Shi, J. Dong, S. Lv, Y. Xu, L. Zhu, J. Xiao, X. Xu, H. Wu, D. Li, Y. Luo and Q. Meng, *Appl. Phys. Lett.*, 2014, **104**, 063901.
16. A. Mei, X. Li, L. Liu, Z. Ku, T. Liu, Y. Rong, M. Xu, M. Hu, J. Chen, Y. Yang, M. Grätzel and H. Han, *Science*, 2014, **345**, 295-298.
17. V. W. Bergmann, S. A. L. Weber, F. Javier Ramos, M. K. Nazeeruddin, M. Grätzel, D. Li, A. L. Domanski, I. Lieberwirth, S. Ahmad and R. Berger, *Nat. Commun.*, 2014, **5**.
18. T. Leijtens, G. E. Eperon, S. Pathak, A. Abate, M. M. Lee and H. J. Snaith, *Nat. Commun.*, 2013, **4**.
19. E. Mosconi, E. Ronca and F. De Angelis, *J. Phys. Chem. Lett.*, 2014, **5**, 2619-2625.
20. P. Schulz, E. Edri, S. Kirmayer, G. Hodes, D. Cahen and A. Kahn, *Energy Environ. Sci.*, 2014, **7**, 1377-1381.
21. E. J. Juarez-Perez, M. Wuβler, F. Fabregat-Santiago, K. Lakus-Wollny, E. Mankel, T. Mayer, W. Jaegermann and I. Mora-Sero, *J. Phys. Chem. Lett.*, 2014, **5**, 680-685.
22. L. Kavan, N. Tétreault, T. Moehl and M. Grätzel, *J. Phys. Chem. C*, 2014, **118**, 16408-16418.
23. T. Moehl, J. H. Im, Y. H. Lee, K. Domanski, F. Giordano, S. M. Zakeeruddin, M. I. Dar, L.-P. Heiniger, M. K. Nazeeruddin, N.-G. Park and M. Grätzel, *J. Phys. Chem. Lett.*, 2014, **5**, 3931-3936.
24. P. Yang, H. Yan, S. Mao, R. Russo, J. Johnson, R. Saykally, N. Morris, J. Pham, R. He and H. J. Choi, *Adv. Funct. Mater.*, 2002, **12**, 323-331.
25. Q. Zhang, C. S. Dandeneau, X. Zhou and G. Cao, *Adv. Mater.*, 2009, **21**, 4087-4108.
26. Ü. Özgür, Y. I. Alivov, C. Liu, A. Teke, M. A. Reshchikov, S. Doğan, V. Avrutin, S.-J. Cho and H. Morkoç, *J. Appl. Phys.*, 2005, **98**, 041301.
27. D. Liu and T. L. Kelly, *Nat. Photonics*, 2014, **8**, 133-138.
28. X. Dong, H. Hu, B. Lin, J. Ding and N. Yuan, *Chem. Commun.*, 2014, **50**, 14405-14408.
29. L. Liang, Z. Huang, L. Cai, W. Chen, B. Wang, K. Chen, H. Bai, Q. Tian and B. Fan, *ACS Appl. Mater. Interfaces*, 2014, **6**, 20585-20589.
30. Y. Natsume and H. Sakata, *Thin Solid Films*, 2000, **372**, 30-36.
31. J. Anderson and G. V. d. W. Chris, *Rep. Prog. Phys.*, 2009, **72**, 126501.
32. S. K. Hau, Y.-J. Cheng, H.-L. Yip, Y. Zhang, H. Ma and A. K. Y. Jen, *ACS Appl. Mater. Interfaces*, 2010, **2**, 1892-1902.
33. L. Zuo, Z. Gu, T. Ye, W. Fu, G. Wu, H. Li and H. Chen, *J. Am. Chem. Soc.*, 2015, **137**, 2674-2679.
34. H. J. Snaith, A. Abate, J. M. Ball, G. E. Eperon, T. Leijtens, N. K. Noel, S. D. Stranks, J. T.-W. Wang, K. Wojciechowski and W. Zhang, *The Journal of Physical Chemistry Letters*, 2014, **5**, 1511-1515.
35. J. Song, E. Zheng, J. Bian, X.-F. Wang, W. Tian, Y. Sanehira and T. Miyasaka, *J. Mater. Chem. A*, 2015, **3**, 10837-10844.
36. J. Song and S. Lim, *J. Phys. Chem. C*, 2007, **111**, 596-600.
37. S. S. Lo, T. Mirkovic, C.-H. Chuang, C. Burda and G. D. Scholes, *Adv. Mater.*, 2011, **23**, 180-197.
38. C. Cheng, A. Amini, C. Zhu, Z. Xu, H. Song and N. Wang, *Sci Rep*, 2014, **4**.
39. F. Kayaci, S. Vempati, C. Ozgit-Akgun, I. Donmez, N. Biyikli and T. Uyar, *Nanoscale*, 2014, **6**, 5735-5745.
40. S.-J. Roh, R. S. Mane, S.-K. Min, W.-J. Lee, C. D. Lokhande and S.-H. Han, *Appl. Phys. Lett.*, 2006, **89**, 253512.
41. V. Manthina, J. P. Correa Baena, G. Liu and A. G. Agrios, *The Journal of Physical Chemistry C*, 2012, **116**, 23864-23870.
42. S.-S. Kim, J.-H. Yum and Y.-E. Sung, *Sol. Energ. Mat. Sol. C.*, 2003, **79**, 495-505.
43. S. Wu, H. Han, Q. Tai, J. Zhang, B. L. Chen, S. Xu, C. Zhou, Y. Yang, H. Hu and X.-Z. Zhao, *Appl. Phys. Lett.*, 2008, **92**, 122106.
44. M. Xiao, F. Huang, W. Huang, Y. Dkhissi, Y. Zhu, J. Etheridge, A. Gray-Weale, U. Bach, Y.-B. Cheng and L. Spiccia, *Angew. Chem. Int. Ed.*, 2014, **126**, 10056-10061.
45. S. M. Sze and K. K. Ng, *Physics of semiconductor devices*, John Wiley & Sons, Third edn., 2006.
46. J. Yang, B. D. Siempelkamp, E. Mosconi, F. De Angelis and T. L. Kelly, *Chem. Mater.*, 2015, **27**, 4229-4236.
47. B. C. O'Regan, S. Scully, A. C. Mayer, E. Palomares and J. Durrant, *J. Phys. Chem. B*, 2005, **109**, 4616-4623.

48. A. Dualeh, T. Moehl, N. Tétreault, J. Teuscher, P. Gao, M. K. Nazeeruddin and M. Grätzel, *ACS Nano*, 2014, **8**, 362-373.
49. H.-S. Kim, I. Mora-Sero, V. Gonzalez-Pedro, F. Fabregat-Santiago, E. J. Juarez-Perez, N.-G. Park and J. Bisquert, *Nat. Commun.*, 2013, **4**.

Graphical Abstract

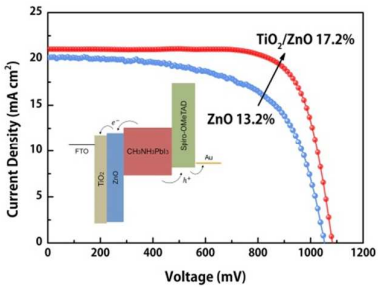

A TiO_2/ZnO bilayer was applied in planar perovskite solar cells to achieve high power-conversion efficiency more than 17%.